AGU PUBLICATIONS

Global Biogeochemical Cycles

RESEARCH ARTICLE
10.1002/2016GB005482

Key Points:
- DOM composition varies across Arctic rivers in northern Alaska
- Parent material and ground ice content drive spatial patterns of DOM
- DOC concentration and aromaticity are negatively correlated with watershed active layer thickness

Supporting Information:
- Supporting Information S1
- Table S1
- Table S2

Correspondence to:
J. A. O'Donnell,
jaodonnell@nps.gov

Citation:
O'Donnell, J. A., G. R. Aiken, D. K. Swanson, S. Panda, K. D. Butler, and A. P. Baltensperger (2016), Dissolved organic matter composition of Arctic rivers: Linking permafrost and parent material to riverine carbon, *Global Biogeochem. Cycles*, *30*, 1811–1826, doi:10.1002/2016GB005482.

Received 16 JUL 2016
Accepted 22 NOV 2016
Accepted article online 24 NOV 2016
Published online 19 DEC 2016

Dissolved organic matter composition of Arctic rivers: Linking permafrost and parent material to riverine carbon

Jonathan A. O'Donnell[1], George R. Aiken[2], David K. Swanson[3], Santosh Panda[4], Kenna D. Butler[2], and Andrew P. Baltensperger[3]

[1]Arctic Network, National Park Service, Anchorage, Alaska, USA, [2]National Research Program, U.S. Geological Survey, Boulder, Colorado, USA, [3]Arctic Network, National Park Service, Fairbanks, Alaska, USA, [4]Geophysical Institute, University of Alaska Fairbanks, Fairbanks, Alaska, USA

Abstract Recent climate change in the Arctic is driving permafrost thaw, which has important implications for regional hydrology and global carbon dynamics. Permafrost is an important control on groundwater dynamics and the amount and chemical composition of dissolved organic matter (DOM) transported by high-latitude rivers. The consequences of permafrost thaw for riverine DOM dynamics will likely vary across space and time, due in part to spatial variation in ecosystem properties in Arctic watersheds. Here we examined watershed controls on DOM composition in 69 streams and rivers draining heterogeneous landscapes across a broad region of Arctic Alaska. We characterized DOM using bulk dissolved organic carbon (DOC) concentration, optical properties, and chemical fractionation and classified watersheds based on permafrost characteristics (mapping of parent material and ground ice content, modeling of thermal state) and ecotypes. Parent material and ground ice content significantly affected the amount and composition of DOM. DOC concentrations were higher in watersheds underlain by fine-grained loess compared to watersheds underlain by coarse-grained sand or shallow bedrock. DOC concentration was also higher in rivers draining ice-rich landscapes compared to rivers draining ice-poor landscapes. Similarly, specific ultraviolet absorbance ($SUVA_{254}$, an index of DOM aromaticity) values were highest in watersheds underlain by fine-grained deposits or ice-rich permafrost. We also observed differences in hydrophobic organic acids, hydrophilic compounds, and DOM fluorescence across watersheds. Both DOC concentration and $SUVA_{254}$ were negatively correlated with watershed active layer thickness, as determined by high-resolution permafrost modeling. Together, these findings highlight how spatial variations in permafrost physical and thermal properties can influence riverine DOM.

1. Introduction

Soils of the northern permafrost region store large amounts of organic carbon (C) that will be subject to mobilization and transport upon warming and thawing of permafrost [*Hugelius et al*., 2014; *Schuur et al*., 2015]. A significant fraction of the permafrost C pool may be released as either carbon dioxide or methane to the atmosphere [*Olefeldt et al*., 2013; *Schädel et al*., 2016], which may function to accelerate rates of warming (i.e., permafrost carbon feedback) [e.g., *Koven et al*., 2011]. The flux of organic C in rivers draining watersheds in the northern permafrost region is also a critical component of the Arctic C budget [*McGuire et al*., 2009, 2010] and anticipated to change under projected warming scenarios [*Frey and Smith*, 2005; *Kicklighter et al*., 2013]. While considerable advancements have been made in recent years to better constrain the timing and magnitude of the permafrost carbon feedback [*Koven et al*., 2015; *Schuur et al*., 2015], uncertainties remain regarding the lateral transport and fate of dissolved organic carbon (DOC) released from permafrost soils [*Kicklighter et al*., 2013]. These uncertainties are due in part to complex interactions among physical (hydrology and soil thermal dynamics), chemical (DOC biolability and photolability), and biological drivers (microbial constraints on DOC production and mineralization) [*Cory et al*., 2014; *Spencer et al*., 2015; *Vonk et al*., 2015; *Walvoord et al*., 2012].

Permafrost thaw and subsequent changes to watershed hydrology and biogeochemistry vary across space and time. The vulnerability of permafrost to thawing is controlled not only by climate but also by ecosystem properties (soil properties and drainage), which can determine the thermal and hydraulic properties of soils [*Shur and Jorgenson*, 2007; *Jorgenson et al*., 2010]. Recent work by *Jorgenson et al*. [2013] illustrated that spatial variation in parent material (coarse-grained versus fine-grained deposits) and ground ice content

(ice-rich versus ice-poor permafrost) are strong determinants of postthaw soil drainage and soil C storage. These factors may also influence the amount and composition of DOC in rivers. Many field studies of DOC export have focused efforts in ice-rich and C-rich landscapes, such as Pleistocene yedoma deposits [e.g., *Vonk et al*., 2013] or permafrost peatlands [e.g., *Olefeldt and Roulet*, 2012], given the potential for large C cycle feedbacks from these landscapes to the climate system [e.g., *Koven et al*., 2011]. However, ice-poor permafrost (e.g., bedrock and ice-poor glacial deposits) with lower C storage is common across the Arctic [*Ping et al*., 2008; *Hugelius et al*., 2014]. Postthaw hydrology and subsequent transfer of C from soil to rivers are likely to vary across watersheds underlain by different soil types and prethaw ground ice contents [*O'Donnell et al*., 2012, 2014] and should also be considered to better constrain DOC fluxes and fate from the northern permafrost region.

Chemical characterization of the riverine dissolved organic matter (DOM) in high-latitude watersheds is useful for understanding organic matter source, biolability and photolability, and ultimate fate under warming and thawing of permafrost [*Cory et al*., 2014; *Spencer et al*., 2015; *Vonk et al*., 2015]. In the present study, we characterized dissolved organic matter (DOM) in 70 rivers draining heterogeneous landscapes across a broad region in northern Alaska, and we characterized study watersheds using three different approaches. First, we classified watersheds into six broad parent material classes (bedrock-loess, bedrock-glacial, glaciolacustrine, loess, sand, and volcanic deposits) and ground ice categories (high-, moderate-, and low-ice contents) using ecological mapping and remotely sensed imagery. Second, we quantified watershed areas comprising organic-dominated landscapes, carbonate barrens, and noncarbonate mineral lithology using ecotype and geological mapping. Third, we estimated permafrost thermal state (i.e., active layer thickness (ALT) and mean annual soil temperature (MAST)) for each watershed using output from a permafrost thermal model [*Panda et al*., 2015]. To evaluate the effects of these landscape characteristics on DOM composition, we measured bulk DOC concentration, major DOM chemical fractions, and DOM optical properties (UV-visible absorbance and fluorescence) on all river samples.

2. Methods

2.1. Study Region

We sampled 69 streams and rivers within or adjacent to National Park Service (NPS) units of the Arctic Inventory and Monitoring Network in northern Alaska between 2013 and 2015 (Figure 1 and Tables 1 and S1 in supporting information). The Arctic Network consists of five park units, including Bering Land Bridge National Preserve, Cape Krusenstern National Monument, Gates of the Arctic National Park and Preserve, Kobuk Valley National Park, and Noatak National Preserve, and covers more than 8×10^6 ha. The study area includes most of the central and western Brooks Range, with elevations ranging from sea level up to 2500 m. Vegetation is dominated by arctic tundra, boreal spruce (*Picea mariana* and *Picea glauca*), and birch (*Betula papyrifera*) [*Jorgenson et al*., 2009]. Tall and low shrubs are common along river floodplains, hillslope drainage ways, and near treeline [*Swanson*, 2015] and have generally expanded in abundance throughout the region in recent decades [*Tape et al*., 2006].

Climate in the study region is variable, with mean annual air temperatures ranging from −5°C in lowlands and to the south, and −10°C in highlands and to the north [*PRISM Climate Group*, 2009]. Mean annual precipitation ranges from 30 to 40 cm in western and southern lowlands and 40 to 75 cm in highlands. Since 1950, mean annual air temperature has increased by 1.5 to 1.7°C, with most of the warming concentrated in the winter months [*Stafford et al*., 2000]. Nearly the entire study region is located in the continuous permafrost zone, where >90% of the land area is underlain by permafrost. Permafrost-associated land features are common throughout the region, including polygonal ground and thermokarst lakes [*Hopkins*, 1949; *Jones et al*., 2011], pingos [*Wetterich et al*., 2012], solifluction lobes [*Hamilton*, 2010], active layer detachment slides, and retrogressive thaw slumps [*Swanson*, 2014; *Balser et al*., 2014].

2.2. Watershed and Landscape Analyses

2.2.1. Parent Material and Ground Ice Classification

For each stream, we delineated watershed areas upstream of the sampling location using the Watershed Boundary Dataset within the U.S. Geological Survey's National Hydrography Dataset (NHD; http://nhd.usgs.gov). For a subset of watersheds, we delineated and digitized watersheds by eye using a 63 K topographic map in ArcMap 10.3 geographic information systems software (http://www.esri.com). Dominant parent

Figure 1. Map of river study sites in five NPS units in Arctic Alaska. Sites varied by parent material and ground ice content. The background imagery is from the National Land Cover Database (http://www.mrlc.gov/).

material types were described for each watershed based on surface geology maps [*Hamilton*, 2010] and/or ecological subsection maps. Ecological subsection maps were previously developed for all five NPS units of the Arctic Network (Figure 1) [*Boggs and Michaelson*, 2001; *Jorgenson*, 2001; *Jorgenson et al.*, 2002; *Swanson*, 2001a, 2001b] and were designed to reflect ecologically significant regions based on land cover (i.e., vegetation), permafrost and periglacial landforms, and bedrock and surface geology. Using these maps and the citations therein, watersheds were then classified into one of six dominant parent material classes: (1) bedrock-loess, (2) bedrock-glacial, (3) glaciolacustrine, (4) loess, (5) sand, and (6) volcanic deposits (Figure 2).

Ground ice content is spatially heterogeneous across the study region, and its volume is closely linked to soil-forming factors, quaternary history, and modes of permafrost aggradation [*Kanevskiy et al.*, 2011]. We used ecological subsection maps [*Boggs and Michaelson*, 2001; *Jorgenson*, 2001; *Jorgenson et al.*, 2002; *Swanson*, 2001a, 2001b] and satellite imagery (IKONOS; http://www.geoeye.com) to classify watersheds into three primary ground ice categories. High-ice watersheds were typically located in flat, low-lying regions with thick fine-grained sedimentary deposits (e.g., Pleistocene loess deposits or yedoma) [*Strauss et al.*, 2013], where ground ice volumes typically exceed 20% [*Olefeldt et al.*, 2016]. Ice-rich terrain was also observed in watersheds underlain primarily by thick peat deposits and sand (Ahnewetut Creek) and volcanic ash deposits (Killuk River). High-ice watersheds typically contain a vast spatial extent of surface features, such as polygonal ground [*Swanson*, 2016] and thermokarst lakes, which indicate the presence of either massive ice (e.g., wedge ice) or extensive segregated-ice volumes (Figures 2g and 2h). Moderate-ice watersheds typically have ground ice volumes ranging from 10 to 20% [*Olefeldt et al.*, 2016] and were observed at sites underlain by comparatively thinner glaciolacustrine deposits. Retrogressive thaw slumps were commonly observed in this region (Figure 2i) [*Swanson*, 2014]. Low-ice sites have less than 10% ground ice by volume and were common in bedrock-dominated watersheds (bedrock-glacial and bedrock-loess), where little to no thermokarst features were present at the ground surface.

Table 1. Study Sites and Watershed Classifications

Watershed Name/*Parent Material Class*	Watershed Area (ha)	Latitude (°N)	Longitude (°W)	Parent Material Class	Ground Ice Class	Carbonate Area (%)	Noncarbonate Mineral Area (%)	Organic Area (%)
Bering Land Bridge National Preserve								
Espenberg River	205	66.558	−164.016	Loess	High	0.0	28.7	58.8
Fairhaven Ditch	53	65.721	−163.081	Volcanic	Low	0.0	46.5	52.8
Goodhope River	87	65.798	−163.620	Bedrock-loess	Moderate	0.0	53.7	46.0
Killuk River	280	66.562	−164.412	Volcanic	High	0.0	34.1	53.3
Kugruk River	123	65.567	−162.928	Volcanic	Low	0.0	62.2	34.4
Kuzitrin River	862	65.425	−164.135	Loess	High	1.2	58.7	37.6
Noxopaga River	954	65.521	−164.161	Volcanic	Moderate	19.7	34.9	43.7
Nugnugaluktuk River	585	66.198	−164.249	Loess	High	21.2	0.0	69.2
Pish River	365	66.125	−164.009	Loess	High	6.0	31.1	60.0
Serpentine River	742	66.086	−165.217	Loess	High	7.5	36.4	53.9
Cape Krusenstern National Monument								
Agagrak River	38	67.526	−163.971	Bedrock-glacial	Low	5.5	62.5	32.0
Jade Creek	103	67.425	−163.784	Loess	High	7.4	57.6	34.5
Kilikmak Creek	184	67.350	−163.739	Bedrock-glacial	Low	10.6	42.3	46.3
New Heart Creek	50	67.606	−164.106	Bedrock-glacial	Moderate	7.0	32.2	48.4
Omikviorok River	368	67.680	−164.103	Bedrock-glacial	Moderate	6.2	44.3	48.7
Rabbit Creek	369	67.470	−163.771	Bedrock-loess	Low	4.1	68.5	27.2
Situkuyok River	183	67.116	−163.309	Bedrock-glacial	Low	34.5	38.7	26.5
Umagatsiak Creek	22	67.541	−163.991	Bedrock-glacial	Low	14.0	39.6	46.4
Gates of the Arctic National Park and Preserve								
Alatna River	7948	66.614	−152.621	Bedrock-glacial	Low	15.2	72.6	8.0
April Creek	567	67.979	−154.489	Bedrock-glacial	Low	0.2	81.3	8.3
Easter Creek	1056	68.123	−154.129	Bedrock-glacial	Low	2.0	74.6	18.0
Glacier River	875	67.348	−150.679	Bedrock-glacial	Low	40.9	47.1	9.3
Hammond River	583	67.553	−150.051	Bedrock-glacial	Low	33.1	57.4	6.1
Itkillik River	312	68.150	−150.241	Bedrock-glacial	Low	7.4	77.7	0.8
John River	5341	67.153	−151.834	Bedrock-glacial	Low	21.6	63.8	11.0
Killik River	2799	68.156	−154.159	Bedrock-glacial	Low	0.8	79.2	13.0
Kobuk River Headwaters	257	67.240	−154.064	Bedrock-glacial	Low	18.6	68.7	4.5
Middle Fork Koyukuk River	3288	67.076	−150.550	Bedrock-glacial	Low	20.8	65.4	9.8
North Fork Koyukuk River	3894	67.310	−150.708	Bedrock-glacial	Low	22.1	62.7	10.0
Tinayguk River	968	67.581	−151.064	Bedrock-glacial	Low	17.9	63.7	12.4
Kobuk Valley National Park								
Ahnewetut Creek	110	67.168	−158.783	Sand	High	0.0	42.6	55.0
Akillik River	1619	67.201	−158.572	Bedrock-loess	High	6.4	74.3	19.0
Elaroniluk Creek	61	67.043	−159.834	Bedrock-glacial	Low	6.6	68.2	24.8
Kaligurichearк River	428	67.193	−159.274	Sand	Low	0.5	80.5	19.0
Kallarichuk River	475	67.106	−159.741	Bedrock-loess	Low	0.0	85.0	15.0
Kavet Creek	90	67.128	−159.034	Sand	Low	0.0	84.9	15.1
Nigeruk Creek	79	67.183	−159.302	Loess	High	0.0	58.1	41.5
Salmon River	1743	67.154	−159.460	Bedrock-loess	Low	6.7	76.1	17.1
Tutuksuk River	923	67.190	−159.345	Bedrock-loess	Low	8.1	77.6	14.3
Noatak National Preserve								
Agashashok Mainstem 1	753	67.474	−162.225	Bedrock-glacial	Low	38.2	25.0	36.7
Agashashok Mainstem 2	1025	67.268	−162.636	Bedrock-glacial	Low	32.8	29.4	37.8
Agashashok Mainstem Trib 1	3	67.490	−162.177	Bedrock-glacial	Low	38.3	46.1	15.5
Agashashok Mainstem Trib 3	38	67.483	−162.215	Bedrock-glacial	Low	22.0	32.0	46.0
Agashashok Mainstem Trib 4	9	67.475	−162.234	Bedrock-glacial	Low	24.5	64.5	11.0
Agashashok Northfork 1	130	67.608	−161.747	Bedrock-loess	Low	44.2	24.8	30.9
Agashashok Northfork 2	394	67.490	−162.109	Bedrock-glacial	Low	23.1	42.9	34.0
Agashashok Northfork Trib 1	38	67.606	−161.749	Bedrock-loess	Low	24.1	28.1	47.8
Agashashok Northfork Trib 2	14	67.569	−161.886	Bedrock-glacial	Low	0.7	61.7	37.5
Agashashok Northfork Trib 3	10	67.545	−161.963	Bedrock-glacial	Low	10.1	56.2	33.7
Agashashok Northfork Trib 4	95	67.522	−162.060	Bedrock-glacial	Low	35.7	35.3	28.9
Agashashok Southfork 1	61	67.545	−161.681	Bedrock-loess	Low	96.5	0.0	3.5
Agashashok Southfork 2	302	67.481	−162.129	Bedrock-glacial	Low	51.6	8.3	40.1
Agashashok Southfork Trib 1	12	67.545	−161.681	Bedrock-loess	Low	92.4	0.0	7.6
Agashashok Southfork Trib 2	26	67.498	−161.871	Bedrock-glacial	Low	61.5	0.0	38.5
Agashashok Southfork Trib 3	37	67.464	−161.977	Bedrock-glacial	Low	81.4	0.0	18.6

Table 1. (continued)

Watershed Name/*Parent Material Class*	Watershed Area (ha)	Latitude (°N)	Longitude (°W)	Parent Material Class	Ground Ice Class	Carbonate Area (%)	Noncarbonate Mineral Area (%)	Organic Area (%)
Agashashok Southfork Trib 4	34	67.472	−162.071	Bedrock-glacial	Low	20.5	17.1	62.3
Aklumayuak Creek	697	67.905	−160.269	Bedrock-glacial	Low	15.1	47.9	37.0
Anisak River	1928	68.054	−158.940	Glaciolacustrine	Moderate	4.2	59.6	35.5
Aniuk River	1882	68.007	−157.943	Glaciolacustrine	Moderate	0.6	47.3	51.4
Cutler River	2764	67.845	−158.316	Glaciolacustrine	Moderate	21.5	38.0	40.0
Eli River	761	67.733	−162.420	Glaciolacustrine	Moderate	0.0	61.8	38.1
Imelyak River	1175	67.751	−158.115	Glaciolacustrine	Moderate	34.1	31.3	34.3
Kaluktavik River	907	67.945	−160.957	Bedrock-glacial	Low	1.4	62.4	36.0
Kugururok River	2348	67.996	−161.867	Bedrock-glacial	Moderate	17.6	53.4	28.8
Makpik River	747	68.060	−158.641	Glaciolacustrine	Moderate	0.5	39.1	56.9
Nakolik River	835	67.874	−160.752	Bedrock-glacial	Low	43.8	22.0	34.2
Nanielik Creek	633	68.010	−158.771	Glaciolacustrine	Moderate	35.1	29.5	35.1
Nimiuktuk River	1507	68.150	−159.948	Bedrock-glacial	Low	4.9	66.0	28.5
Sisiak Creek	235	67.911	−160.592	Bedrock-glacial	Low	0.0	52.9	47.0
Uvgoon Creek	141	67.807	−162.347	Bedrock-glacial	Moderate	0.7	37.4	58.5

2.2.2. Watershed Ecotype and Lithology

We used a simple two-step mapping approach to categorize watershed areas into landscape units that were hypothesized to control chemical composition of streams and rivers. First, we used an existing ecological land cover map [*Jorgenson et al*., 2009] to categorize watershed areas into broad groups, defined as organic landscapes, mineral-dominated landscapes, water/snow, and no data/indeterminate (Tables 1 and S2). Organic landscapes generally have organic-horizon thicknesses exceeding 15 cm, shallow active layers, and typically occur in lowland setting with relatively poor drainage. Mineral landscapes generally have relatively thin organic-soil horizons (<10 cm) and thick active layers. Second, the mineral-dominated landscapes were

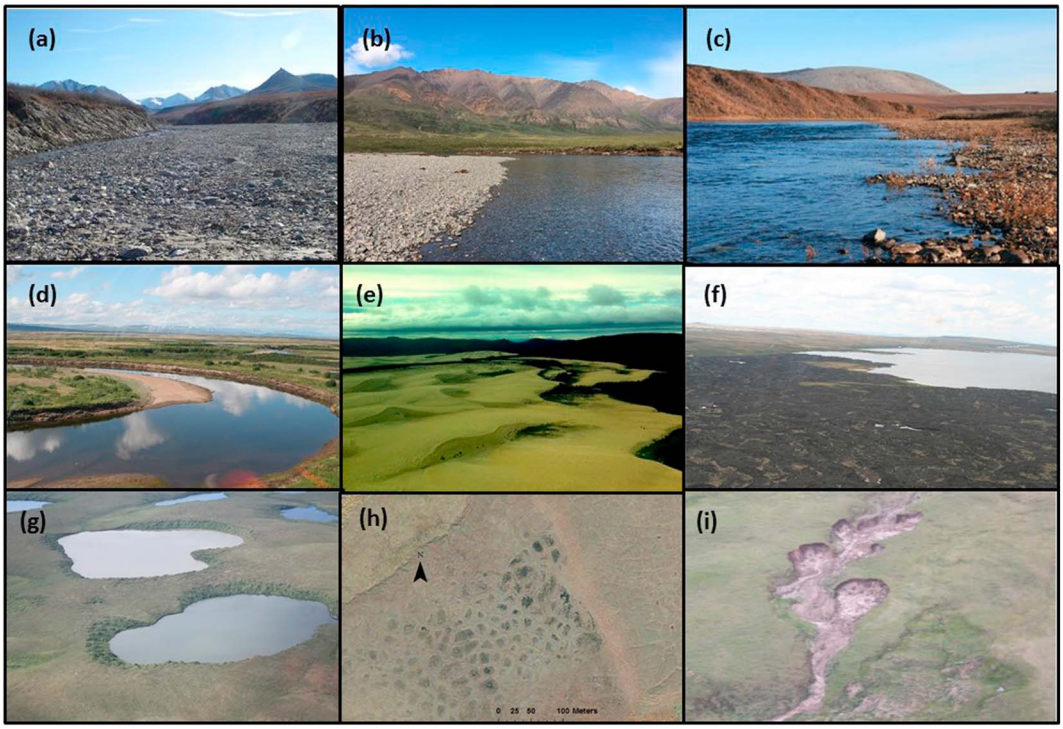

Figure 2. Photographs of six landscape units that vary by dominant parent material: (a) bedrock-loess, (b) bedrock-glacial (coarse-grained), (c) glaciolacustrine (fine-grained), (d) loess (yedoma), (e) sand, and (f) volcanic deposits. Ground ice classes were determined by the extent of features such as (g) thermokarst lakes, (h) polygonal ground, and (i) retrogressive thaw slumps.

further divided into carbonate versus noncarbonate mineral landscapes using a new geologic map of Alaska [*Wilson et al*., 2015]. Carbonate landscapes generally occurred in alpine barren areas and include limestone, dolomite, and metacarbonate lithologies.

2.2.3. Permafrost Modeling

To examine the relationship between soil thermal dynamics and riverine DOM, we used simulated output from the Geophysical Institute Permafrost Laboratory (GIPL) model 1.0 [*Panda et al*., 2015]. GIPL 1.0 is a quasi-transitional, spatially distributed, equilibrium model for calculating MAST at the top of the permafrost table and ALT. The model accounts for the effects of snow, surface vegetation, soil moisture, and soil thermal properties (e.g., thermal conductivity and heat capacity). Ecotype information (e.g., vegetation, physiography, and soil descriptions) from *Jorgenson et al*. [2009] was used as model input data, and thermal parameters were prescribed for each ecotype. The model was driven using downscaled air temperature and precipitation input data from the Scenario Network for Alaska and Arctic Planning [*SNAP*, 2012]. For our analyses, we extracted MAST at the permafrost table and ALT for each watershed using NHD polygons (as described above) for the period 2000–2009.

2.3. DOC Concentrations and DOM Fractionation

All water samples were collected during the open-water period between June and September over 3 years (2013–2015). Samples were collected 25 cm below the surface in a well-mixed location and filtered in situ using a 0.45 μm high-capacity capsule filter connected to a Geopump Series II Peristaltic Pump (Geotech Environmental Equipment, Inc., Denver, CO). Most sites were sampled once, although a number of sites were sampled two or three times during the summer-autumn flow period (June through September), and all samples were treated independently in subsequent analyses. Samples were refrigerated for 7–10 days until analysis at the U. S. Geological Survey organic carbon laboratory in Boulder, CO. DOC concentrations were determined using an O.I. Analytical Model 700 TOC analyzer via the platinum catalyzed persulfate wet oxidation method [*Aiken*, 1992]. A subset of samples was chromatographically separated into different fractions: hydrophobic acids (HPOAs), hydrophilic organic matter (HPI), and transphilic acids (TPIA) using Amberlite XAD-8 and XAD-4 resins [*Aiken et al*., 1992]. The resins preferentially adsorb different classes of organic acids based on aqueous solubility and molecular weight of the solute, chemical composition of the resin, resin surface area, and resin pore size. The amount of organic matter within each fraction, expressed as a percentage of the total DOC concentration, was calculated using the DOC concentration and the sample mass of each fraction. On average, we captured 94% of the total DOC pool through this procedure, and the standard deviation for the mass percentages of the fractionation was ±2%. Isolation of the HPOA fraction was carried out using the lyophilization procedure described in *Spencer et al*. [2010].

2.4. DOM Optical Properties

UV-visible absorbance was measured on filtered river samples and XAD fractions at room temperature using a quartz cell with a path length of 1 cm on an Agilent Model 8453 photodiode array spectrophotometer. Specific UV absorbance ($SUVA_{254}$) was determined for all filtered samples and for major chemical fractions (HPOA, TPIA, and HPI) by dividing the decadal UV-visible absorption coefficient per meter at $\lambda = 254$ nm by DOC concentration. $SUVA_{254}$, which is typically used as an index of DOC aromaticity, provides an "average" absorptivity at $\lambda = 254$ nm for the DOC [*Weishaar et al*., 2003]. $SUVA_{254}$ is reported in units of L mg C^{-1} m^{-1}. *Weishaar et al*. [2003] also showed that UV absorbance values could be biased high by the presence of iron (Fe). To account for potential effects of Fe on UV absorbance, we measured total Fe concentrations on a subset of samples and applied correction factors based on experimental work by *Poulin et al*. [2014]. In general, we observed that the Fe-based correction of UV-Visible absorbance accounted for less than 5% of total CDOM absorbance.

Spectral slope (S) was calculated by fitting an exponential equation to the absorption spectra between 275–295 and 350–400 nm using

$$\alpha_g(\lambda) = \alpha_g(\lambda_{\text{ref}})e^{-S(\lambda-\lambda_{\text{ref}})} \quad (1)$$

where $\alpha_g(\lambda)$ is the Naperian absorption coefficient of CDOM at a specified wavelength, λ_{ref} is a reference wavelength, and S is the slope fitting parameter [*Helms et al*., 2008; *Spencer et al*., 2008]. The spectral slope of the 275–295 nm region ($S_{275-295}$) has been shown to be negatively correlated with the molecular weight of DOM [*Helms et al*., 2008]. Prior studies have shown the spectral slope between 275 and 295 nm ($S_{275-295}$) to

be sensitive to changes in DOM source (e.g., riverine versus estuarine versus open ocean and composition) [*Spencer et al*., 2007].

Fluorescence excitation-emission matrices (EEMs) were measured on filtered river samples and HPOA fractions at room temperature using a Jobin-Yvon Horiba Fluoromax-3 fluorometer. Samples were diluted to minimize inner filter effects with deionized water, when necessary, to a UV absorbance at $\lambda = 254$ nm of 0.2 absorbance units (1 cm cell). Using a 5 nm slit width, EEMs were collected over an excitation range of 240–450 nm every 5 nm and an emission range of 300–600 nm every 2 nm. Scans were corrected for instrument optics, inner filter corrected, Raman area normalized, Raman normalized blank subtracted, and multiplied by the dilution factor if necessary [*Murphy et al*., 2010] and are reported in Raman Units (RUs).

We used a "peak-picking" approach to analyze fluorescence intensities across rivers draining watersheds underlain by different parent material and ground ice contents. We focused on four fluorescence peaks common in aquatic DOM. The A peak, which originates below an excitation maximum of 260 nm and an emission maxima of 448–480 nm, is common in wetland and forested ecosystems and has been described as humic like [*Coble et al*., 1998; *Fellman et al*., 2010]. The C peak is also humic like and originates between excitation maxima of 320–360 nm and an emission maxima of 420–460 nm. The B peak originates between excitation maxima of 270–275 nm and emission maxima of 304–312 and is associated with simple phenols and fluoresces in the same region as the amino acid tyrosine [*Hernes et al*., 2009; *Aiken*, 2014; *Wünsch et al*., 2015]. The T peak originates between excitation maxima of 270–280 nm and emission maxima of 330–368 and has been associated with indole fluorophores, and because it fluoresces in the same region as tryptophan, is commonly referred to as tryptophan like or protein like.

2.5. Data Analysis

All statistical analyses were conducted in R (https://www.r-project.org). We used one-way analysis of variance (ANOVA) to evaluate the separate effects of parent material and the effects of ground ice class on DOM composition. We did not test for interactive effects using two-way ANOVA, because parent material and ground ice often covaried (e.g., all loess sites had high ground ice content). Tukey's Honest Significant Difference (HSD) post hoc test was conducted to compare differences across treatment means. Diagnostics revealed that DOC concentration and $S_{275-295}$ did not meet the assumption of normality and were therefore log transformed. Pearson correlations were used to evaluate relationships among landscape variables (carbonate, noncarbonate, and organic areas), permafrost characteristics (ALT, MAST, and ground ice class), and DOM parameters (DOC concentration, $SUVA_{254}$, and $S_{275-295}$). We also conducted linear regression analysis to examine relationships between landscape variables, permafrost characteristics, and DOM parameters.

3. Results

3.1. Effects of Parent Material on Permafrost Characteristics

Permafrost characteristics (ALT, MAST, and ground ice class) varied across watersheds underlain by different parent materials (Table 2). ALT was deepest in sand-dominated watersheds (mean = 126 ± 29 cm) and was shallowest in loess-dominated watersheds (61 ± 3 cm; Table 2). ALT averaged 69 ± 1 cm and 76 ± 3 cm in bedrock-glacial and bedrock-loess watersheds, respectively. MASTs at the top of the permafrost table were generally warmer in sand-dominated watersheds in the Kobuk River basin (mean = −2.3 ± 1.0°C) and coldest in glaciolacustrine-dominated watersheds (mean = −5.3 ± 1.2°C) in the Noatak River basin. Parent material and ground ice class were closely linked across watersheds. With very few exceptions, nearly all bedrock-glacial ($n = 34$ of 38) and bedrock-loess watersheds ($n = 8$ of 10) were classified as having low-ice content (Table 2). All glaciolacustrine watersheds ($n = 7$) were classified as having moderate-ice content, and all loess-dominated watersheds ($n = 8$) were classified as having high-ice content. However, we observed some variability in ground ice content in watersheds underlain by sand and volcanic deposits, with both high-ice and low-ice conditions observed within these classes. Volcanic deposits include both bedrock-like lava flows, which are typically ice poor, and volcanic ash, which functions more like loess and can be ice rich.

3.2. Effects of Parent Material and Ground Ice on DOM

River and stream (referred to subsequently as river or riverine) DOC concentration varied across watersheds underlain by different parent materials (one-way ANOVA, $F = 12.23$, d.f. = 5, $P < 0.001$) and ground ice class ($F = 13.35$, d.f. = 2, $P < 0.001$; Figure 3). Rivers draining watersheds dominated by loess and volcanic deposits

Table 2. Permafrost Characteristics Across Parent Material Classes[a]

Parent Material Class	Mean ALT (m)	Mean Annual Soil Temp	Ground Ice Class Sample Size (High/Moderate/Low)	Carbonate Area (%)	Noncarbonate Area (%)	Organic Area (%)
Bedrock-glacial	69 ± 1	−3.7 ± 1.1	0/4/60	25 ± 3	44 ± 3	30 ± 2
Bedrock-loess	76 ± 3	−3.9 ± 0.5	1/1/15	44 ± 10	30 ± 9	26 ± 3
Glaciolacustrine	63 ± 3	−5.3 ± 1.2	0/7/0	14 ± 6	44 ± 5	42 ± 3
Loess	61 ± 3	−3.1 ± 0.6	8/0/0	3 ± 1	44 ± 6	49 ± 5
Sand	126 ± 29	−2.3 ± 1.0	1/0/2	0 ± 0	69 ± 13	30 ± 13
Volcanic deposit	63 ± 3	−3.0 ± 0.1	1/1/2	5 ± 5	44 ± 7	46 ± 4

[a]Values are means ± one standard error.

generally had the highest DOC concentrations, averaging 10.1 ± 2.7 and 7.4 ± 2.1 mg C L^{-1}, respectively (Figure 3a). Bedrock- and sand-dominated watersheds had the lowest river DOC concentrations, with mean values ranging from 1.5 to 3.1 mg C L^{-1}. Watersheds underlain by high-ice contents had significantly higher riverine DOC concentrations (mean = 8.2 ± 2.0 mg C L^{-1}) than watersheds classified as moderate or low ice (mean = 2.6 ± 0.3, collectively; Tukey's HSD: $P < 0.001$; Figure 3b).

$SUVA_{254}$ values in river water also varied across watersheds underlain by different parent materials ($F = 8.23$, d.f. = 5, $P < 0.001$) and ground ice class ($F = 17.2$, d.f. = 2, $P < 0.001$; Figure 3). Watersheds underlain by loess and volcanic deposits had the highest $SUVA_{254}$ values, averaging 3.4 ± 0.3 and 3.2 ± 0.3 L mg C^{-1} m^{-1}, respectively, whereas bedrock-dominated watersheds had the lowest $SUVA_{254}$ values (mean <2.2 L mg C^{-1} m^{-1}; Figure 3c). $SUVA_{254}$ values generally increased with watershed ground ice content, ranging from 2.2 ± 0.1 L mg C^{-1} m^{-1} in

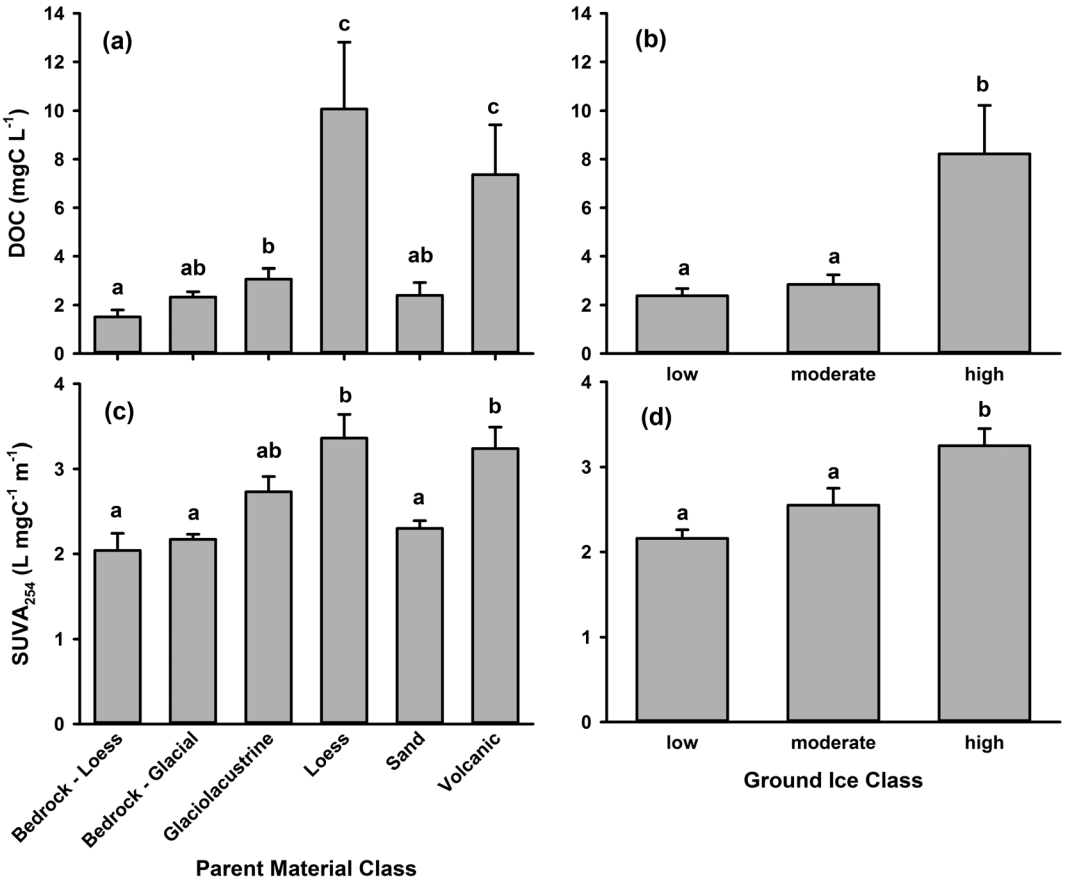

Figure 3. Mean DOC concentration and $SUVA_{254}$ values in rivers draining watersheds with different underlying (a, c) parent materials and (b, d) ground ice categories. Error bars represent one standard error.

watersheds classified as low ice up to 3.3 ± 0.2 L mg C^{-1} m^{-1} in watersheds classified as high ice (Figure 3d). $S_{275-295}$ did not vary significantly across watersheds underlain by different parent material ($P > 0.05$) or ground ice content ($P > 0.05$).

DOM chemical fractions were also variable in rivers draining watersheds underlain by different parent materials and ground ice contents (Figure 4). HPOA comprised the largest fraction of DOM across all rivers, but varied with parent material type, ranging from $36 \pm 4\%$ in sand-dominated watersheds to 52% in a watershed underlain by volcanic deposits (Figure 4a). The HPI fraction was also variable across parent material types, ranging from $16 \pm 1\%$ in glaciolacustrine watersheds to $25 \pm 1\%$ in watersheds underlain by sand. The TPIA fraction was less variable, averaging $21 \pm 3\%$ across all study sites. On average, the HPOA fraction was highest in watersheds classified as high ice ($50 \pm 2\%$) or moderate ice ($48 \pm 6\%$) and lowest in watersheds classified as low ice ($38 \pm 4\%$; Figure 4b). By contrast, the HPI fraction was highest in watersheds classified as low ice ($23 \pm 1\%$) compared to the watersheds classified as moderate or high ice.

We also observed variability in fluorescence characteristics in rivers draining watersheds underlain by different parent material types and ground ice amounts (Figures 5 and S1–S7). The A and C fluorescence peaks were ubiquitous but varied in intensity across river samples (Figure 5). For instance, DOC-normalized fluorescence intensities (in RU) for the A peak region were higher at the ice-rich, loess site Nigeruk Creek (0.20 RU; Figure 5a) compared to bedrock-dominated Agashashok River (0.13 RU; Figure 5b). The B peak was commonly observed in river samples underlain by bedrock, such as the Agashashok watershed (Figure 5b). The protein-like T peak was also common in bedrock-dominated and glaciolacustrine watersheds (Figures 5b and 5c) but was largely absent from loess-dominated watersheds.

3.3. Ecotype and Permafrost Controls on Riverine Carbon

River DOC concentrations were significantly, positively correlated to organic area in each watershed, described by the linear regression equation $y = 0.01x - 0.12$ ($R^2 = 0.41$, $P < 0.0001$; Figure 6a). Despite varying considerably across and within parent material classes, organic area was generally highest in watersheds underlain by loess and volcanic deposits (Table 1). River DOC concentrations were also significantly negatively correlated with mean ALT for each watershed, described by the equation $y = -1.69x + 1.46$ ($R^2 = 0.38$, $P < 0.0001$; Figure 6b). $SUVA_{254}$ was also positively correlated with organic area, described by the equation $y = 0.02x + 1.57$ ($R^2 = 0.25$, $P < 0.0001$). Similarly, $SUVA_{254}$ was also negatively correlated with mean ALT, described by the equation $y = -2.5x + 4$ ($R^2 = 0.12$, $P = 0.0004$). $S_{275-295}$ was significantly negatively correlated to carbonate area ($r = -0.77$, $P = 0.03$; Table 3). We did not observe any significant correlations between DOM parameters and MAST at the top of the permafrost.

4. Discussion

4.1. Permafrost Controls on Watershed Hydrology and DOM

Landscape characteristics are important controls on the concentration and flux of DOC in high-latitude watersheds [*Ågren et al.*, 2007; *Buffam et al.*, 2007; *Harms et al.*, 2016]. The influence of permafrost extent on river DOC concentrations has been documented in prior studies [*Maclean et al.*, 1999; *Carey*, 2003; *Frey and Smith*, 2005]. DOM composition in rivers has also been linked to seasonal changes in thaw depth [*Neff et al.*, 2006], interannual increases in active layer thickness [*O'Donnell et al.*, 2014], permafrost controls on groundwater discharge [*O'Donnell et al.*, 2012], watershed permafrost extent [*Olefeldt et al.*, 2014], and thermokarst [*Abbott et al.*, 2014; *Spencer et al.*, 2015]. Our analyses here expand upon this work by documenting the importance of spatial variations in permafrost soil characteristics, including parent material, ground ice, ecotype, and soil thermal state, on the amount and composition of DOC in Arctic rivers.

In general, we observed high DOC concentrations in rivers draining watersheds underlain by fine-grained deposits, with shallow active layers, and a large fraction of the watershed characterized as organic ecotypes. Fine-grained deposits, such as loess silt and volcanic ash, typically have low hydraulic conductivity [*Koch et al.*, 2013], reducing soil-water infiltration and drainage. Poorly drained soils foster the development of thick organic-soil horizons, which store large amounts of organic carbon [*Trumbore and Harden*, 1997]. Further, these thick organic-soil horizons insulate permafrost soils from warm summer air temperatures [*Shur and Jorgenson*, 2007]. Spatial variations in organic-horizon thickness are closely and negatively linked to active layer thickness [*O'Donnell et al.*, 2009]. Together, these factors facilitate the lateral movement of water

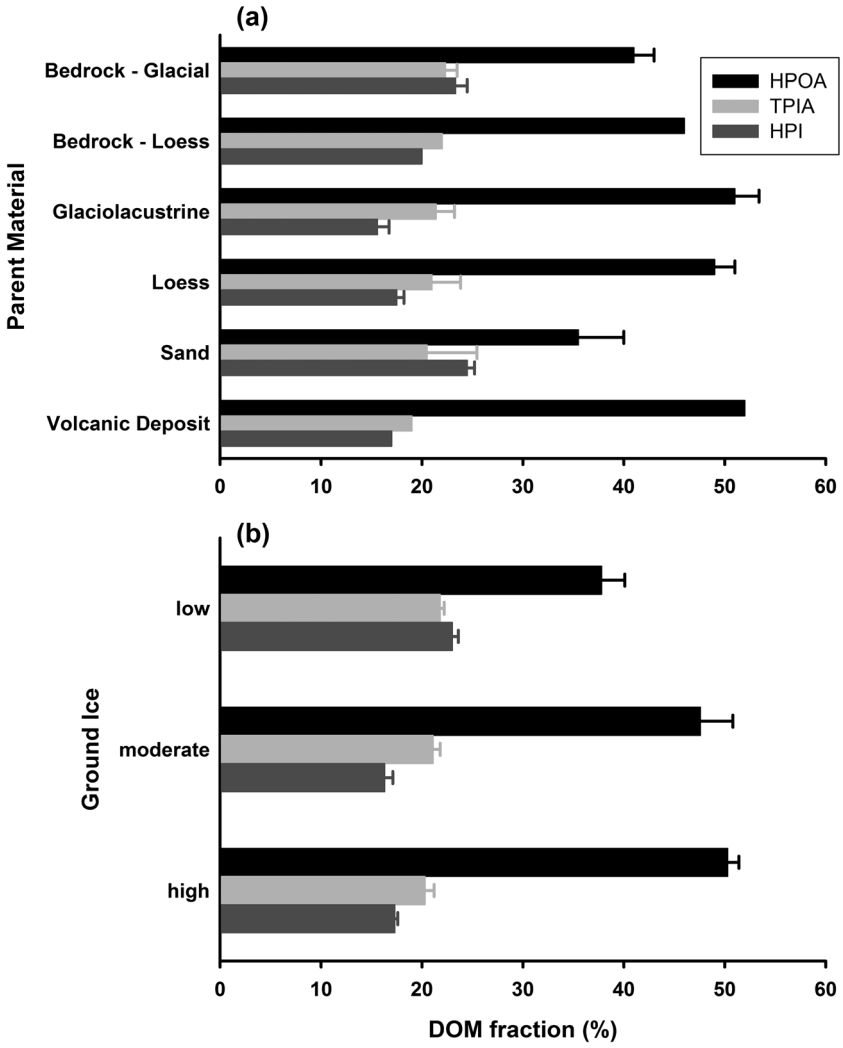

Figure 4. Mean percentages of major DOM fractions in rivers draining watersheds underlain by (a) different dominant parent materials and (b) different ground ice contents. HPOA = hydrophobic organic acids, TPIA = transphilic organic acids, and HPI = hydrophilic organic matter.

through C-rich horizons of the active layer and subsequent transport of DOC from soils to rivers. DOM aromaticity, as determined by $SUVA_{254}$ measurements, was highest in watersheds underlain by loess or volcanic ash. DOM leached from organic-soil horizons of the active layer tends to be highly aromatic [*Wickland et al*., 2007; *O'Donnell et al*., in review] and is a large source of DOM to rivers underlain by fine-grained deposits like loess [*O'Donnell et al*., 2010; *Mann et al*., 2012].

Rivers draining watersheds underlain by coarse-grained deposits or shallow bedrock, with deeper active layers, and with a larger fraction of mineral-dominated landscapes generally had lower DOC concentrations. Coarse-grained deposits (e.g., sand and glacial till) and fractured bedrock can foster high soil-water infiltration rates and enhanced soil drainage compared to fine-grained deposits. These well-drained and oxygenated soils facilitate rapid turnover of C inputs, leading to minimal organic C accumulation in organic-soil horizons [*Pastick et al*., 2014]. Deeper active layers in these watersheds are driven both by the thinner organic-soil horizons and also higher thermal conductivity of coarse-grained deposits and bedrock when compared to fine-grained deposits like silt. Together, these characteristics influence river DOC concentration by driving deeper groundwater flows through C-poor deposits or bedrock. DOM was less aromatic in these rivers, which is consistent with prior work documenting the relationship between $SUVA_{254}$ and groundwater discharge to sub-Arctic rivers [*O'Donnell et al*., 2012].

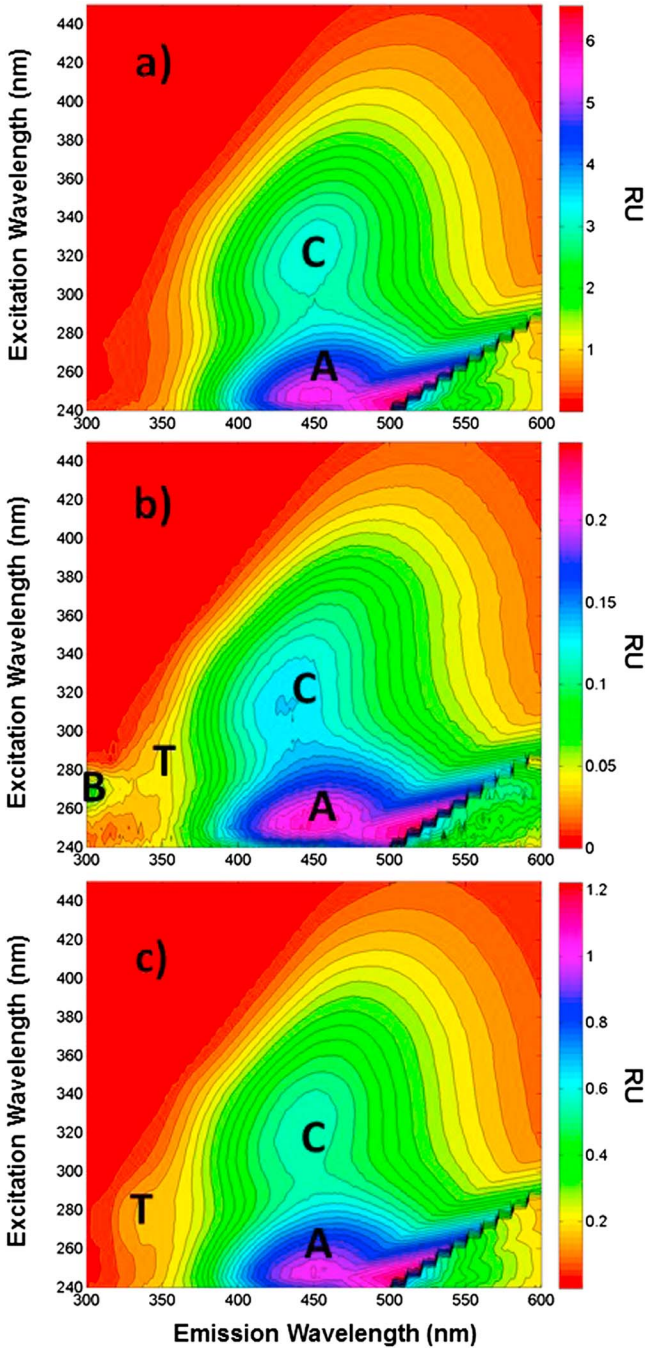

Figure 5. Representative excitation-emission matrices (EEMs) from three rivers draining watersheds with different parent materials and ground ice contents: (a) Nigeruk Creek (ice-rich loess), (b) Agashashok River (ice-poor bedrock), and (c) Makpik River (moderate ice and glaciolacustrine). The uppercase letters represent different fluorescence peaks. A and C peaks are humic-like fluorophores, B peak is a simple phenol associated with amino acid tyrosine, and T peak is a tryptophan-like indole.

4.2. Implications of DOM Composition for Reactivity

Hydrophobic organic acids were the dominant fraction in rivers across all parent material and ground ice classes (Figure 4), which is common in many high-latitude watersheds [*Michaelson et al.*, 1998; *Striegl et al.*, 2005; *O'Donnell et al.*, 2010]. We did observe spatial variation in the HPOA fraction across watersheds underlain by different parent materials, which likely reflects the combined effects of soil organic matter source, and microbial and physical transformation of the DOM pool. Aquatic fulvic acids dominate the HPOA fraction and are generated primarily from the microbial degradation of plant and moss litter in soils [*McKnight and Aiken*, 1998]. HPOA comprised a larger fraction of DOM in watersheds underlain by fine-grained deposits, where poorly drained soils with thick organic-soil horizons contribute large amounts of HPOA to rivers. HPOA comprised a lower proportion of DOM in watersheds underlain by coarse-grained deposits and bedrock, which was likely driven by permafrost configuration and subsequent effects on subsurface hydrology. Longer transit times through deep subsurface flow paths may allow for higher mineralization of the HPOA fraction [*O'Donnell et al.*, 2012]. More specifically, the HPOA fraction can be preferentially stabilized through sorption to reactive mineral surfaces, reducing its concentration in aquatic ecosystems [*Kaiser et al.*, 1996]. In watersheds where permafrost is thawing or has thawed, the rerouting of subsurface flows through unfrozen mineral soils may stabilize HPOA [*Kawahigashi et al.*, 2006], reducing HPOA and DOC concentrations in Arctic rivers [*Kawahigashi et al.*, 2004; *Striegl et al.*, 2005].

Hydrophilic compounds (HPI) generally followed the opposite pattern of HPOA across watersheds, comprising a larger fraction in watersheds underlain by coarse-grained deposits and shallow bedrock. Spatial variation in HPI is likely influenced by groundwater discharge. In the Yukon River basin, HPI comprised a larger fraction of DOM with increasing groundwater discharge to rivers [*O'Donnell et al.*, 2012]. Prior studies have documented a

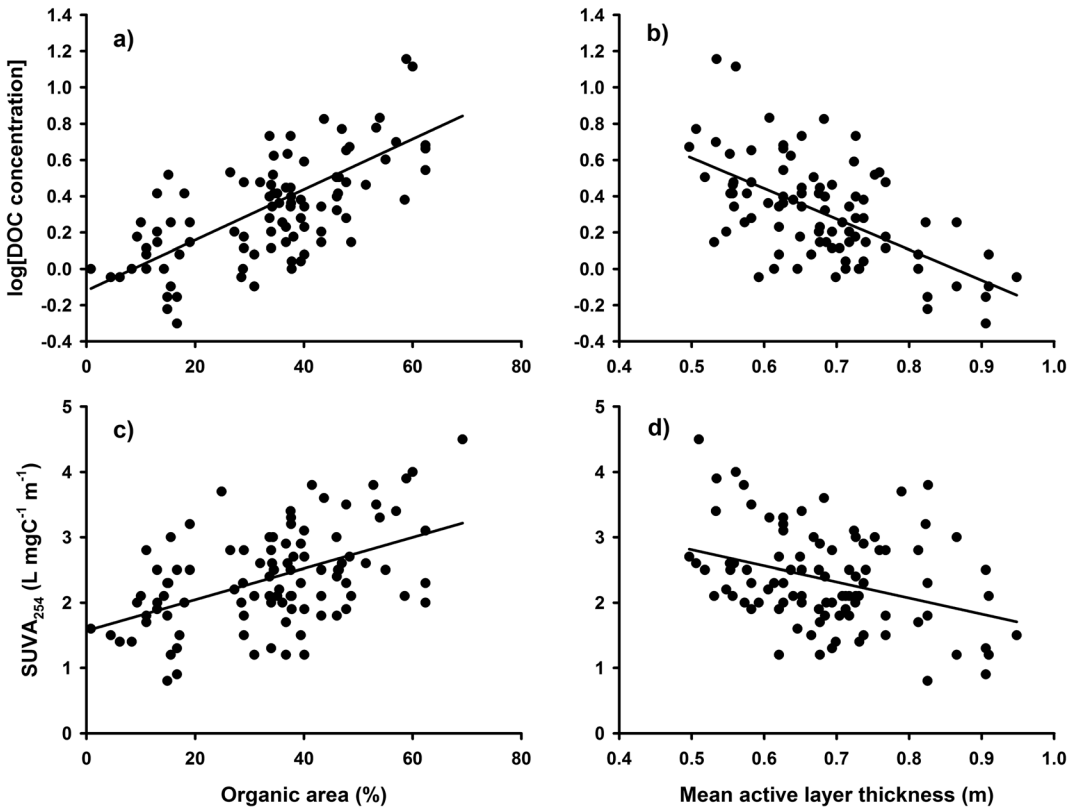

Figure 6. Linear regressions relating DOC concentration and $SUVA_{254}$ to organic area and mean active layer thickness.

strong relationship between HPI and DOC biolability in high-latitude ecosystems [*Qualls and Haines*, 1991; *Michaelson et al*., 1998], as a portion of HPI is composed of low-molecular-weight hydrophilic compounds. While some permafrost types (e.g., yedoma) deposits store large amounts of ancient low-molecular-weight organic acids, such as acetate [*Ewing et al*., 2015], it is not likely that we are measuring ancient DOM in these middle-order to high-order rivers [*Aiken et al*., 2014]. Upon thaw, ancient biolabile DOM is rapidly mineralized in headwater streams [*Drake et al*., 2015; *Spencer et al*., 2015; *Mann et al*., 2015] and generally has not been detected in higher-order watersheds downstream of thermokarst features [*Aiken et al*., 2014]. However, DOM fluorescence data across rivers indicate higher protein-like fluorescence intensities in watersheds underlain by coarse-grained deposits, which have been associated with higher rates of DOC mineralization [e.g., *Balcarczyk et al*., 2009]. Protein-like fluorescence components are typically higher in streams where flow is generated by deeper groundwater flow paths compared to streamflow generated by shallow subsurface flows [*O'Donnell et al*., 2012, 2014].

Table 3. Pearson Correlation Matrix for Ecotype, Permafrost, and DOC Variables[a]

	Carbonate Area	Noncarbonate Mineral Area	Organic Area	Mean ALT	Mean Ground Temperature	DOC	$SUVA_{254}$	$S_{275-295}$
Carbonate area	-	***−0.85***	−0.37	***0.77***	0.38	−0.59	−0.69	***−0.77***
Noncarbonate mineral area		-	−0.18	−0.42	−0.47	0.19	0.30	0.60
Organic area			-	−0.68	0.14	***0.76***	***0.75***	0.37
Mean ALT				-	0.45	−0.66	***−0.75***	***−0.70***
Mean ground temperature					-	0.05	−0.07	−0.36
DOC concentration						-	***0.93***	0.65
$SUVA_{254}$							-	***0.81***
$S_{275-295}$								-

[a]All *r* correlation coefficients in bold and italics are statistically significant at $P < 0.05$.

4.3. Landscape Vulnerability to Thaw and Impacts on DOC

Our findings relating landscape and permafrost characteristics (parent material, ground ice content, and soil thermal dynamics) to riverine DOC reflect present-day permafrost state, which is largely stable in the region [*Panda et al*., 2015]. Our observations provide insight to the degree to which permafrost exerts influence on watershed hydrology, patterns of soil C accumulation, and DOM transport. However, permafrost warming and thawing is projected for much of the study region by 2100 across a range of climate scenarios [*Panda et al*., 2015], which will likely have profound consequences for Arctic ecosystems and biogeochemical cycling. Spatial variation in ground ice content will likely mediate the magnitude of these impacts, with the largest impacts projected in ice-rich landscapes [*Olefeldt et al*., 2016]. We did observe a significant effect of ground ice on DOC concentration and DOM composition, which likely reflected the effects of ice on hydraulic properties of soils and subsurface hydrology. The fate of DOC under projected permafrost thaw will depend both upon historic patterns of C accumulation in permafrost soils and landscape changes associated with thawing of ice-rich terrain.

Soil-forming factors (climate, topography, and parent material) and permafrost aggradation mode (syngenetic versus epigenetic) are important determinants of C storage and ground ice volumes in soils [*Jenny*, 1941; *Jorgenson et al*., 2013] and consequently will affect the magnitude of DOC released to rivers upon thaw. For instance, during the late Pleistocene, high rates of loess deposition in unglaciated regions facilitated widespread burial and stabilization of C and syngenetic aggradation of massive ice wedges and segregated ice (i.e., yedoma) [*Kanevskiy et al*., 2011]. Permafrost in bedrock-dominated soils formed epigenetically (in the absence of sedimentation), and thus, soils underlain by shallow bedrock store less C [*Ping et al*., 2008; *Hugelius et al*., 2014] and are typically ice poor [*Jorgenson et al*., 2013]. Coarse-grained deposits like sand can form permafrost through either epigenetic or syngenetic processes but generally store less C than loess [*Johnson et al*., 2011].

Ground ice distributions determine the vulnerability of Arctic and sub-Arctic landscapes to thermokarst [*Jorgenson and Osterkamp*, 2005; *Jorgenson et al*., 2010; *Olefeldt et al*., 2016]. In ice-rich terrain, thermokarst results in the subsidence of the ground surface, which can dramatically alter hydrologic networks, erosion and sedimentation, vegetation, and C export to rivers [*Fourtier et al*., 2007; *Abbott et al*., 2014]. In ice-poor terrain, the effects of permafrost thaw will be minimal with respect to disturbance of the ground surface and thermal erosion [*Jorgenson and Osterkamp*, 2005]. Still, we observed a significant relationship between active layer thickness and both DOC concentration and DOM aromaticity, an observation that spans both ice-rich terrain and ice-poor terrain. This finding suggests that permafrost thaw, through a gradual thickening of the active layer, will still influence the amount and composition of DOM release to rivers in the future.

Acknowledgments

We thank two anonymous reviewers and Josh Koch for providing helpful comments on the manuscript. We also thank Sara Breitmeyer for helping with DOM analyses. The National Park Service Inventory and Monitoring Program provided funding for this study. The U.S. Geological Survey's National Research Program and Changing Arctic Ecosystems program provided additional support. Any use of trade, firm, or product names is for descriptive purposes only and does not imply endorsement by the U.S. Government. George Aiken and Kenna Butler did not materially contribute to the model application described in this publication. Most data can be accessed via the National Park Service's Integrated Resource Management Application (IRMA) website (https://irma.nps.gov) or by contacting the authors directly.

References

Abbott, B. W., J. R. Larouche, J. B. Jones Jr., W. B. Bowden, and A. W. Balser (2014), Elevated dissolved organic carbon biodegradability from thawing and collapsing permafrost, *J. Geophys. Res. Biogeosci.*, *119*, 2049–2063, doi:10.1002/2014JG002678.

Ågren, A., I. Buffam, M. Jansson, and H. Laudon (2007), Importance of seasonality and small streams for the landscape regulation of dissolved organic carbon export, *J. Geophys. Res.*, 112, G03003, doi:10.1029/2006JG000381.

Aiken, G. R. (1992), Chloride interference in the analysis of dissolved organic carbon by the wet oxidation method, *Environ. Sci. Technol.*, *26*, 2435–2439, doi:10.1021/es00036a015.

Aiken, G. R. (2014), Fluorescence and dissolved organic matter: A chemist's perspective, in *Aquatic Organic Matter Fluorescence*, edited by P. G. Cole et al., pp. 35–74, Cambridge Univ. Press, Cambridge, U. K.

Aiken, G. R., D. M. McKnight, K. A. Thorn, and E. M. Thurman (1992), Isolation of hydrophilic organic acids from water using nonionic macroporous resins, *Org. Geochem.*, *4*, 567–573.

Aiken, G. R., R. G. M. Spencer, R. G. Striegl, P. F. Schuster, and P. A. Raymond (2014), Influences of glacier melt and permafrost thaw on the age of dissolved organic carbon in the Yukon River basin, *Global Biogeochem. Cycles*, *28*, 525–537, doi:10.1002/2013GB004764.

Balcarczyk, K. L., J. B. Jones Jr., R. Jaffe, and N. Maie (2009), Stream dissolved organic matter bioavailability and composition underlain with discontinuous permafrost, *Biogeochemistry*, *94*, 255–270, doi:10.1007/s10533-009-93240-x.

Balser, A. W., J. B. Jones, and R. Gens (2014), Timing of retrogressive thaw slump initiation in the Noatak Basin, northwestern Alaska, USA, *J. Geophys. Res. Earth Surf.*, *119*, 1106–1120, doi:10.1002/2013JF002889.

Boggs, K., and J. Michaelson (2001), *Ecological Subsections of Gates of the Arctic National Park and Preserve*, 84 pp., Alaska Region, National Park Service.

Buffam, I., H. Laudon, J. Temnerud, C. M. Mörth, and K. Bishop (2007), Landscape-scale variability of acidity and dissolved organic carbon during spring flood in a boreal stream network, *J. Geophys. Res.*, *112*, G01022, doi:10.1029/2006JG000218.

Carey, S. K. (2003), Dissolved organic carbon fluxes in a discontinuous permafrost subarctic alpine catchment, *Permafrost Periglac. Process.*, *14*, 161–171, doi:10.1002/ppp.444.

Coble, P. G., C. E. Del Castillo, and B. Avril (1998), Distribution and optical properties of CDOM in the Arabian Sea during the 1995 Southwest Monsoon, *Deep Sea Res., Part II*, *45*, 2195–2223, doi:10.1016/S0967-0645(98)00068-X.

Cory, R. M., C. P. Ward, B. C. Crump, and G. W. Kling (2014), Sunlight controls water column processing of carbon in arctic fresh waters, *Science*, *345*, 925–928, doi:10.1126/science.1253119.

Drake, T. W., K. P. Wickland, R. G. M. Spencer, D. M. McKnight, and R. G. Striegl (2015), Ancient low-molecular-weight organic acids in permafrost fuel rapid carbon dioxide production upon thaw, *Proc. Natl. Acad. Sci. U. S. A.*, *112*, 13,946–13,951, doi:10.1073/pnas1511705112.

Ewing, S. A., J. A. O'Donnell, G. R. Aiken, K. Butler, D. Butman, L. Windham-Myers, and M. Z. Kanevskiy (2015), Long-term anoxia and release of ancient, labile carbon upon thaw of Pleistocene permafrost, *Geophys. Res. Lett.*, *42*, 107,30–107,38, doi:10.1002/2015GL066296.

Fellman, J. B., E. Hood, and R. G. M. Spencer (2010), Fluorescence spectroscopy opens new windows into dissolved organic matter dynamics in freshwater ecosystems: A review, *Limnol. Oceanogr.*, *55*, 2452–2462, doi:10.4319/lo.2010.55.6.2452.

Fourtier, D., M. Allard, and Y. Shur (2007), Observation of rapid drainage system development by thermal erosion of ice wedges on Bylot Island, Canadian Arctic Archipelago, *Permafrost Periglac. Process.*, *18*, 229–243, doi:10.1002/ppp.595.

Frey, K. E., and L. C. Smith (2005), Amplified carbon release from vast West Siberian peatlands by 2100, *Geophys. Res. Lett.*, *32*, L09401, doi:10.1029/2004GL022025.

Hamilton, T. D. (2010), Surficial geologic map of the Noatak National Preserve, Alaska, U.S. Geological Survey Scientific Investigations Map, 3036, 1 sheet, scale 1:250,000, 1 pamphlet, p. 21.

Harms, T. K., J. W. Edmonds, H. Genet, I. F. Creed, D. Aldred, A. Balser, and J. B. Jones (2016), Catchment influence on nitrate and dissolved organic matter in Alaskan streams across a latitudinal gradient, *J. Geophys. Res. Biogeosci.*, *121*, 350–369, doi:10.1002/2015JG003201.

Helms, J. R., A. Stubbins, J. D. Ritchie, E. C. Minor, D. J. Kieber, and K. Mopper (2008), Absorption spectral slopes and slope ratios as indicators of molecular weight, source, and photobleaching of chromophoric dissolved organic matter, *Limnol. Oceanogr.*, *53*, 955–969, doi:10.4319/lo.2008.53.3.0955.

Hernes, P. J., B. A. Bergamaschi, R. S. Eckard, and R. G. M. Spencer (2009), Fluorescence-based proxies for lignin in freshwater dissolved organic matter, *J. Geophys. Res.*, 114, G00F03, doi:10.1029/2009JG000938.

Hopkins, D. M. (1949), Thaw lakes and thaw sinks in the Imuruk Lake Area, Seward Peninsula, *J. Geol.*, *57*, 119–131.

Hugelius, G., et al. (2014), Estimated stocks of circumpolar permafrost carbon with quantified uncertainty ranges and identified data gaps, *Biogeosciences*, *11*, 6573–6593, doi:10.5194/bg-11-6573-2014.

Jenny, H. (1941), *Factors of Soil Formation: A System of Quantitative Pedology*, 281 pp., McGraw Hill, New York.

Johnson, K. D., et al. (2011), Soil carbon distribution in Alaska in relation to soil-forming factors, *Geoderma*, *167-168*, 71–84, doi:10.1016/j.geoderma.2011.10.006.

Jones, B. M., G. Grosse, C. D. Arp, M. C. Jones, K. M. Walter Anthony, and V. E. Romanovsky (2011), Modern thermokarst lake dynamics in the continuous permafrost zone, northern Seward Peninsula, Alaska, *J. Geophys. Res.*, *116*, G00M03, doi:10.1029/2011JG001666.

Jorgenson, M. T. (2001), Landscape-level mapping of ecological units for the Bering Land Bridge National Preserve, p. 76, Report prepared for the National Park Service.

Jorgenson, M. T., and T. E. Osterkamp (2005), Response of boreal ecosystems to varying modes of permafrost degradation, *Can. J. For. Res.*, *35*, 2100–2111, doi:10.1139/X05-153.

Jorgenson, M. T., D. K. Swanson, and M. Macander (2002), *Landscape-Level Mapping of Ecological Units for the Noatak National Preserve, Alaska*, 73 pp., National Park Service, Inventory and Monitoring Program, Alaska.

Jorgenson, M. T., J. E. Roth, P. F. Miller, M. J. Macander, M. S. Duffy, A. F. Wells, G. V. Frost, and E. R. Pullman (2009), An ecological land survey and landcover map of the Arctic Network, Natural Resource Technical Report NPS/ARCN/NRTR–2009/270, National Park Service, Fort Collins, Colo.

Jorgenson, M. T., V. Romanovsky, J. Harden, Y. Shur, J. O'Donnell, E. A. G. Schuur, M. Kanevskiy, and S. Marchenko (2010), Resilience and vulnerability of permafrost to climate change, *Can. J. For. Res.*, *40*, 1219–1236, doi:10.1139/x10-060.

Jorgenson, M. T., J. Harden, M. Kanevskiy, J. O'Donnell, K. Wickland, S. Ewing, K. Manies, Q. Zhuang, Y. Shur, and Q. Zhuang (2013), Reorganization of vegetation, hydrology, and soil carbon after permafrost degradation across heterogeneous boreal landscapes, *Environ. Res. Lett.*, *8*, doi:10.1088/1748-9326/8/3/035017.

Kaiser, K., G. Guggenberger, and W. Zech (1996), Sorption of DOM and DOM fractions to forest soils, *Geoderma*, 281–303, doi:10.1016/S0016-7061(96)00071-7.

Kanevskiy, M., Y. Shur, D. Fortier, M. T. Jorgenson, and E. Stephani (2011), Cryostratigraphy of late Pleistocene syngenetic permafrost (yedoma) in northern Alaska, Itkillik River exposure, *Quat. Res.*, *75*, 584–596, doi:10.1016/j.yqres.2010.12.003.

Kawahigashi, M., K. Klaus, K. Kalbitz, A. Rodionov, and G. Guggenberger (2004), Dissolved organic matter in small streams along a gradient from discontinuous to continuous permafrost, *Global Change Biol.*, *10*, 1576–1586, doi:10.1111/j.1365-2486.2004.00827.x.

Kawahigashi, M., K. Kaiser, A. Rodionov, and G. Guggenberger (2006), Sorption of dissolved organic matter by mineral soils of the Siberian forest tundra, *Global Change Biol.*, *12*, 1868–1877, doi:10.1111/j.1365-2486.2006.01203.x.

Kicklighter, D. W., D. J. Hayes, J. W. McClelland, B. J. Peterson, A. D. McGuire, and J. M. Melillo (2013), Insights and issues with simulating terrestrial DOC loading of Arctic river networks, *Ecol. Appl.*, *23*, 1817–1836, doi:10.1890/11-1050.1.

Koch, J. C., S. A. Ewing, R. Striegl, and D. M. McKnight (2013), Rapid runoff via shallow throughflow and deeper preferential flow in a boreal catchment underlain by frozen silt (Alaska, USA), *Hydrogeol. J.*, *21*, 93–106, doi:10.1007/s10040-012-0934-3.

Koven, C. D., B. Ringeval, P. Friedlingstein, P. Ciais, P. Cadule, D. Khvorostyanov, G. Krinner, and C. Tarnocai (2011), Permafrost carbon-climate feedbacks accelerate global warming, *Proc. Natl. Acad. Sci. U. S. A.*, *108*, 14,769–14,774, doi:10.1073/pnas.1103910108.

Koven, C. D., et al. (2015), A simplified, data-constrained approach to estimate the permafrost carbon-climate feedback, *Philos. Trans. R. S. A*, doi:10.1098/rsta.2014.0423.

Maclean, R., M. W. Oswood, J. G. Irons III, and W. H. McDowell (1999), The effect of permafrost on stream biogeochemistry: A case study of two streams in the Alaskan (U.S.A.) taiga, *Biogeochemistry*, *47*, 239–267, doi:10.1007/BF00992909.

Mann, P. J., A. Davydova, N. Zimov, R. G. M. Spencer, S. Davydov, E. Bulygina, S. Zimov, and R. M. Holmes (2012), Controls on the composition and lability of dissolved organic matter in Siberia's Kolyma River basin, *J. Geophys. Res.*, 117, G01028, doi:10.1029/2011JG001798.

Mann, P. J., T. I. Eglinton, C. P. McIntyre, N. Zimov, A. Davydova, J. E. Vonk, R. M. Holmes, and R. G. M. Spencer (2015), Utilization of ancient permafrost carbon in headwaters of Arctic fluvial networks, *Nat. Commun.*, *6*, doi:10.1038/ncomms8856.

McGuire, A. D., L. G. Anderson, T. R. Christensen, S. Dallimore, L. Guo, D. J. Hayes, M. Heimann, T. D. Lorenson, R. W. Macdonald, and N. Roulet (2009), Sensitivity of the carbon cycle in the Arctic to climate change, *Ecol. Monogr.*, *79*, 523–555, doi:10.1890/08-2025.1.

McGuire, A. D., et al. (2010), An analysis of the carbon balance of the Arctic Basin from 1997 to 2006, *Tellus B*, *62*, 455–474, doi:10.1111/j.1600-0889.2010.00497.x.

McKnight, D. M., and G. R. Aiken (1998), Sources and age of aquatic humus, in *Aquatic Humic Substances*, 1st ed., edited by D. Hessen and L. Tranvik, pp. 9–39 , Springer, Berlin.

Michaelson, G. J., C. L. Ping, G. W. Kling, and J. E. Hobbie (1998), The character and bioactivity of dissolved organic matter at thaw and in the spring runoff waters of the arctic tundra north slope, Alaska, *J. Geophys. Res.*, *103*, 28,939–28,946, doi:10.1029/98JD02650.

Murphy, K. R., K. D. Butler, R. G. M. Spencer, C. A. Stedmon, J. R. Boehme, and G. R. Aiken (2010), Measurement of dissolved organic matter fluorescence in aquatic environments: An interlaboratory comparison, *Environ. Sci. Technol.*, *44*, 9405–9412, doi:10.1021/es102362t.

Neff, J. C., J. C. Finlay, S. A. Zimov, S. P. Davydova, J. J. Carrasco, E. A. G. Schuur, and A. I. Davydova (2006), Seasonal changes in the age and structure of dissolved organic carbon in Siberian rivers and streams, *Geophys. Res. Lett.*, 33, L23401, doi:10.1029/2006Gl028222.

O'Donnell, J. A., M. R. Turetsky, J. W. Harden, K. L. Manies, L. E. Pruett, G. Shetler, and J. C. Neff (2009), Interactive effects of fire, soil climate, and moss on CO_2 fluxes in black spruce ecosystems of interior Alaska, *Ecosystems*, *12*, 57–72, doi:10.1007/s10021-008-9206-4.

O'Donnell, J. A., G. R. Aiken, E. S. Kane, and J. B. Jones (2010), Source water controls on the character and origin of dissolved organic matter in streams of the Yukon River basin, Alaska, *J. Geophys. Res.*, 115, G03025, doi:10.1029/2009JG001153.

O'Donnell, J. A., G. R. Aiken, M. A. Walvoord, and K. D. Butler (2012), Dissolved organic matter composition of winter stream flow in the Yukon River basin: Implications of permafrost thaw and increased groundwater discharge, *Global Biogeochem. Cycles*, *26*, GB0E06, doi:10.1029/2012GB004341.

O'Donnell, J. A., G. R. Aiken, M. A. Walvoord, P. A. Raymond, K. D. Butler, M. M. Dornblaser, and K. Heckman (2014), Using dissolved organic matter composition and age to detect permafrost thaw in boreal streams of interior Alaska, *J. Geophys. Res. Biogeosci.*, *119*, 2155–2170, doi:10.1002/2014JG002695.

Olefeldt, D., and N. T. Roulet (2012), Effects of permafrost and hydrology on the composition and transport of dissolved organic carbon in a subarctic peatland complex, *J. Geophys. Res.*, *117*, G01005, doi:10.1029/2011JG001819.

Olefeldt, D., M. R. Turetsky, P. M. Crill, and A. D. McGuire (2013), Environmental and physical controls on northern terrestrial methane emissions across permafrost zones, *Global Change Biol.*, *19*, 589–603, doi:10.1111/gcb.12071.

Olefeldt, D., A. Persson, and M. R. Turetsky (2014), Influence of the permafrost boundary on dissolved organic matter characteristics in rivers within the Boreal and Taiga plains of western Canada, *Environ. Res. Lett.*, *9*, doi:10.1088/1748-9326/9/3/035005.

Olefeldt, D., et al. (2016), Circumpolar distribution and carbon storage of permafrost landscapes, *Nature Commun.*, doi:10.1038/ncomms13043.

Panda, S. K., V. E. Romanovsky, and S. S. Marchenko (2015), Forecast of permafrost distribution, temperature, and active layer thickness for Arctic National Parks of Alaska through 2100, Fall Meeting of the AGU, San Francisco, Calif.

Pastick, N. J., M. Rigge, B. K. Wylie, M. T. Jorgenson, J. R. Rose, K. D. Johnson, and L. Ji (2014), Distribution and landscape controls on organic layer thickness and carbon within the Alaska Yukon River Basin, *Geoderma*, 79–94, doi:10.1016/j.geoderma.2014.04.008.

Ping, C.-L., G. J. Michaelson, M. T. Jorgenson, J. M. Kimble, H. Epstein, V. E. Romanovsky, and D. A. Walker (2008), High stocks of soil organic carbon in the North American Arctic region, *Nat. Geosci.*, *1*, 615–619, doi:10.1038/ngeo284.

Poulin, B. A., J. N. Ryan, and G. R. Aiken (2014), Effects of iron on optical properties of dissolved organic matter, *Environ. Sci. Technol.*, *48*, 10,098–10,106, doi:10.1021/es502670r.

PRISM Climate Group (2009), *July Mean Average Temperature for Alaska 1971–2000, Annual Mean Average Temperature for Alaska 1971–2000*, Oregon State Univ, Corvallis, Oreg.

Qualls, R. G., and B. L. Haines (1991), Biodegradability of dissolved organic matter in forest throughfall, soil solution, and stream water, *Soil Sci. Soc. Am. J.*, *56*, 578–586, doi:10.2136/sssaj1992.03615995005600020038x.

Schädel, C., et al. (2016), Potential carbon emissions dominated by carbon dioxide from thawed permafrost soils, *Nat. Clim. Change*, *6*, 950–953, doi:10.1038/nclimate3054.

Schuur, E. A. G., et al. (2015), Climate change and the permafrost carbon feedback, *Nature*, *520*, 171–179, doi:10.1038/nature14338.

Shur, Y., and M. T. Jorgenson (2007), Patterns of permafrost formation and degradation in relation to climate and ecosystems, *Permafrost Periglac. Process.*, *18*, 7–19, doi:10.1002/ppp.582.

SNAP (Scenarios Network for Alaska and Arctic Planning) (2012), Tools and data. [Available at http://www.snap.uaf.edu/data.php.]

Spencer, R. G. M., B. A. Pellerin, B. A. Bergamaschi, B. D. Downing, T. E. C. Kraus, D. R. Smart, R. A. Dahlgren, and P. J. Hernes (2007), Diurnal variability in riverine dissolved organic matter composition determined by in situ optical measurement in the San Joaquin River (California, USA), *Hydrol. Process*, *21*, 3181–3189, doi:10.1002/hyp.6887.

Spencer, R. G. M., G. R. Aiken, K. P. Wickland, R. G. Striegl, and P. J. Hernes (2008), Seasonal and spatial variability in dissolved organic matter quantity and composition from the Yukon River basin, Alaska, *Global Biogeochem. Cycles*, *22*, GB4002, doi:10.1029/2008GB003231.

Spencer, R. G. M., G. R. Aiken, R. Y. Dyda, K. D. Butler, B. A. Bergamaschi, and P. J. Hernes (2010), Comparison of XAD with other dissolved lignin isolation techniques and a compilation of analytical improvements for the analysis of lignin in aquatic settings, *Organic Geochem.*, *41*, 445–453, doi:10.1016/j.orggeochem.2010.02.004.

Spencer, R. G. M., P. J. Mann, T. Dittmar, T. I. Eglinton, C. McIntyre, R. M. Holmes, N. Zimov, and A. Stubbins (2015), Detecting the signature of permafrost thaw in Arctic rivers, *Geophys. Res. Lett.*, *42*, 2830–2835, doi:10.1002/2015GL063498.

Stafford, J. M., G. Wendler, and J. Curtis (2000), Temperature and precipitation of Alaska: 50 year trend analysis, *Theor. Appl. Climatol.*, *67*, 33–44, doi:10.1007/s007040070014.

Strauss, J., L. Schirrmeister, G. Grosse, S. Wetterich, M. Ulrich, U. Herzschuh, and H. W. Hubberten (2013), The deep permafrost carbon pool of the Yedoma region in Siberia and Alaska, *Geophys. Res. Lett.*, *40*, 6165–6170, doi:10.1002/2013GL058088.

Striegl, R. G., G. R. Aiken, M. M. Dornblaser, P. A. Raymond, and K. P. Wickland (2005), A decrease in discharge-normalized DOC export by the Yukon River during summer through autumn, *Geophys. Res. Lett.*, 32, L21413, doi:10.1029/2005GL024413.

Swanson, D. K. (2001a), *Ecological Subsections of Cape Krusenstern National Monument*, 27 pp., National Park Service – Alaska Region, Inventory and Monitoring Program, Anchorage, Alaska.

Swanson, D. K. (2001b), *Ecological Subsections of Kobuk Valley National Park*, 49 pp., National Park Service – Alaska Region, Inventory and Monitoring Program, Anchorage, Alaska.

Swanson, D. K. (2014) Mapping of erosion features related to thaw of permafrost in the NPS Arctic Inventory and Monitoring Network, Alaska, Natural Resource Technical Report NPS/ARCN/NRTR—2014/912, National Park Service. Fort Collins, Colo.

Swanson, D. K. (2015), Environmental limits of tall shrubs in Alaska's Arctic National Parks, *PLoS One*, *10*, e0138387, doi:10.1371/journal.pone.0138387.

Swanson, D. K. (2016), Stability of ice-wedges in Kobuk Valley National Park and the Noatak National Preserve, Natural Resource Report NPS/ARCN/NRR – 2016/1248. National Park Service, Fort Collins, Colo.

Tape, K., D. M. Sturn, and C. Racine (2006), The evidence for shrub expansion in Northern Alaska and the Pan-Arctic, *Global Change Biol.*, *12*, 686–702, doi:10.1111/j.1365-2486.2006.01128.x.

Trumbore, S. E., and J. W. Harden (1997), Accumulation and turnover of carbon in organic and mineral soils of the BOREAS northern study area, *J. Geophys. Res.*, *102*, 28,817–28,830, doi:10.1029/97JD02231.

Vonk, J. E., et al. (2013), High biolability of ancient permafrost carbon upon thaw, *Geophys. Res. Lett.*, *40*, 2689–2693, doi:10.1002/grl.50348.

Vonk, J. E., S. E. Tank, P. J. Mann, R. G. M. Spencer, C. C. Treat, R. G. Striegl, B. W. Abbott, and K. P. Wickland (2015), Biodegradability of dissolved organic carbon in permafrost soils and aquatic systems: A meta-analysis, *Biogeosciences*, *12*, 6915–6930, doi:10.5194/bg-12-6915-2015.

Walvoord, M. A., C. I. Voss, and T. P. Wellman (2012), Influence of permafrost distribution on groundwater flow in the context of climate-driven permafrost thaw: Example from Yukon Flats Basin, Alaska, United States, *Water Resour. Res.*, *48*, W07524, doi:10.1029/2011WR011595.

Weishaar, J. L., G. R. Aiken, B. A. Bergamaschi, M. S. Fram, R. Fujii, and K. Mopper (2003), Evaluation of specific ultraviolet absorbance as an indicator of the chemical composition and reactivity of dissolved organic carbon, *Environ. Sci. Technol.*, *37*, 4702–4708, doi:10.1021/es030360x.

Wetterich, S., G. Grosse, L. Schirrmeister, A. A. Andreev, A. A. Borov, F. Kienast, N. H. Bigelow, and M. E. Edwards (2012), Late Quaternary environmental and landscape dynamics revealed by a pingo sequence on the northern Seward Peninsula, Alaska, *Quat. Sci. Rev.*, *39*, 26–44, doi:10.1016/j.quascirev.2012.01.027.

Wickland, K. P., J. C. Neff, and G. R. Aiken (2007), Dissolved organic carbon in Alaskan boreal forest: Sources, chemical characteristics, and biodegradability, *Ecosystems*, doi:10.1007/s10021-007-9101-4.

Wilson, F. H., C. P. Hults, C. G. Mull, and S. M. Karl (2015) Geologic map of Alaska, U. S. Geological Survey Scientific Investigations Map, 3340, pamphlet p. 196, 2 sheets, scale 1:1,584,000, doi:10.3133/sim3340.

Wünsch, U. J., K. R. Murphy, and C. A. Stedmon (2015), Fluorescence quantum yields of natural organic matter and organic compounds: Implications for the fluorescence-based interpretation of organic matter composition, *Front. Mar. Sci.*, doi:10.3389/fmars.2015.00098.